Journal of Organometallic Chemistry 880 (2019) 213–222

Contents lists available at ScienceDirect

Journal of Organometallic Chemistry

journal homepage: www.elsevier.com/locate/jorganchem

Chalcogenide-capped triiron clusters $[Fe_3(CO)_9(\mu_3\text{-}E)_2]$, $[Fe_3(CO)_7(\mu_3\text{-}CO)(\mu_3\text{-}E)(\mu\text{-}dppm)]$ and $[Fe_3(CO)_7(\mu_3\text{-}E)_2(\mu\text{-}dppm)]$ (E = S, Se) as proton-reduction catalysts

Ahibur Rahaman [a], Shishir Ghosh [b, c], Sucharita Basak-Modi [b], Ahmed F. Abdel-Magied [a], Shariff E. Kabir [d], Matti Haukka [e], Michael G. Richmond [f], George C. Lisensky [g], Ebbe Nordlander [a, **], Graeme Hogarth [c, *]

[a] Inorganic Chemistry Research Group, Chemical Physics, Center for Chemistry and Chemical Engineering, Lund University, Box 124, SE-221 00, Lund, Sweden
[b] Department of Chemistry, University College London, 20 Gordon Street, London, WC1H OAJ, UK
[c] Department of Chemistry, King's College London, Britannia House, 7 Trinity Street, London, SE1 1DB, UK
[d] Department of Chemistry, Jahangirnagar University, Savar, Dhaka 1342, Bangladesh
[e] Department of Chemistry, University of Jyvaskyla, Box 111, FI-40014, Jyväskylä, Finland
[f] Department of Chemistry, University of North Texas, 1155 Union Circle, Box 305070, Denton, TX, 76203, USA
[g] Department of Chemistry, Beloit College 700 College St., Beloit, WI, 53511, USA

ARTICLE INFO

Article history:
Received 30 July 2018
Received in revised form
10 October 2018
Accepted 22 October 2018
Available online 25 October 2018

Keywords:
Triiron
Chalcogenide
Cluster
Proton-reduction
Electrochemistry

ABSTRACT

Chalcogenide-capped triiron clusters $[Fe_3(CO)_7(\mu_3\text{-}CO)(\mu_3\text{-}E)(\mu\text{-}dppm)]$ and $[Fe_3(CO)_7(\mu_3\text{-}E)_2(\mu\text{-}dppm)]$ (E = S, Se) have been examined as proton-reduction catalysts. Protonation studies show that $[Fe_3(CO)_9(\mu_3\text{-}E)_2]$ are unaffected by strong acids. Mono-capped $[Fe_3(CO)_7(\mu_3\text{-}CO)(\mu_3\text{-}E)(\mu\text{-}dppm)]$ react with $HBF_4.Et_2O$ but changes in IR spectra are attributed to BF_3 binding to the face-capping carbonyl, while bicapped $[Fe_3(CO)_7(\mu_3\text{-}E)_2(\mu\text{-}dppm)]$ are protonated but in a process that is not catalytically important. DFT calculations are presented to support these protonation studies. Cyclic voltammetry shows that $[Fe_3(CO)_9(\mu_3\text{-}Se)_2]$ exhibits two reduction waves, and upon addition of strong acids, proton-reduction occurs at a range of potentials. Mono-chalcogenide clusters $[Fe_3(CO)_7(\mu_3\text{-}CO)(\mu_3\text{-}E)(\mu\text{-}dppm)]$ (E = S, Se) exhibit proton-reduction at *ca.* -1.85 (E = S) and -1.62 V (E = Se) in the presence of *p*-toluene sulfonic acid (*p*-TsOH). Bicapped $[Fe_3(CO)_7(\mu_3\text{-}E)_2(\mu\text{-}dppm)]$ undergo quasi-reversible reductions at -1.55 (E = S) and -1.45 V (E = Se) and reduce *p*-TsOH to hydrogen but protonated species do not appear to be catalytically important. Current uptake is seen at the first reduction potential in each case, showing that $[Fe_3(CO)_7(\mu_3\text{-}E)_2(\mu\text{-}dppm)]^-$ are catalytically active but a far greater response is seen at *ca.* -1.9 V being tentatively associated with reduction of $[H_2Fe_3(CO)_7(\mu_3\text{-}E)_2(\mu\text{-}dppm)]^+$. In general, selenide clusters are reduced at slightly lower potentials than sulfide analogues and show slightly higher current uptake under comparable conditions.

1. Introduction

Hydrogen is a potentially clean and efficient energy-carrier [1–3]; however, its current synthesis is energy-intensive and uses fossil-fuel resources, while the direct utilization of solar energy for hydrogen production through photocatalytic [4] or photo-electrochemical [5,6] water-splitting is poorly developed. Algae can produce hydrogen and oxygen from water [7] and hydrogenases then act as catalysts for the reversible oxidation of hydrogen to protons and electrons. In the late 1990s, crystal structures of [FeFe]-hydrogenases revealed that the active site consists of a diiron sub-unit with a bridging dithiolate ligand and ancillary CO/CN^- ligands linked to an Fe_4S_4 ferredoxin subunit [8–11]. This generated enormous interest in the development of synthetic analogues of the active site with a wide range of diiron biomimetics being tested as proton-reduction catalysts [12]. Key

* Corresponding author.
** Corresponding author.
E-mail addresses: ebbe.nordlander@chemphys.lu.se (E. Nordlander), graeme.hogarth@kcl.ac.uk (G. Hogarth).

https://doi.org/10.1016/j.jorganchem.2018.10.018
0022-328X/

features of (electro)catalysts for proton reduction include the abilities to bind a proton(s) and undergo facile reduction, both being well-established properties of low-valent transition metal clusters [13]. Hence, clusters with nuclearities of three or greater are promising candidates as catalysts for clean hydrogen formation via proton-reduction [14–27]. Two groups have independently studied proton-reduction by the sulfide cluster $[Fe_3(CO)_9(\mu_3\text{-}S)_2]$ (**1S**) [14,15]. In MeCN with acetic acid, H_2 production takes place at the second reduction potential (−1.75 V), establishing the dianion $[Fe_3(CO)_9(\mu_3\text{-}S)_2]^{2-}$ (**1S^{2-}**) as the catalyst [14]. In the presence of the strong acid $HBF_4.Et_2O$, both mono and dianions are active proton-reduction catalysts at potentials of −1.03 V and −1.30 V, respectively [15]. Since $[Fe_3(CO)_9(\mu_3\text{-}S)_2]$ (**1S**) does not readily protonate even with strong acids, initial reduction is a prerequisite for proton-reduction. Sun, Åkermark and co-workers [16] have explored the proton-reduction activity of the diphosphine-substituted cluster $[Fe_3(CO)_5(\mu_3\text{-}S)_2(\kappa^2\text{-}dppv)_2]$ [dppv = *cis*-1,2-bis(diphenylphosphino)ethylene] that, in contrast, is readily protonated by trifluoromethanesulfonic (triflic) acid and catalyses proton-reduction at -0.98 V in CH_2Cl_2, the first reduction potential of $[(\mu\text{-}H)Fe_3(CO)_5(\mu_3\text{-}S)_2(\kappa^2\text{-}dppv)_2]^+$. In seeking to extend and develop the proton-reduction chemistry of low-valent triiron clusters, we turned our attention to the chalcogenide-capped clusters $[Fe_3(CO)_7(\mu_3\text{-}CO)(\mu_3\text{-}E)(\mu\text{-}dppm)]$ (**2S**, **2Se**) and $[Fe_3(CO)_7(\mu_3\text{-}E)_2(\mu\text{-}dppm)]$ (**3S**, **3Se**) with the expectation that introduction of the diphosphine bis(diphenylphosphino)methane (dppm) may serve to stabilise the relatively fragile triiron core, while also favouring protonation at the triiron centre. Further, the ability to vary the chalcogenide cap potentially allows redox-tuning. Herein we report the electrocatalytic proton-reduction properties of **2** and **3**, as well as $[Fe_3(CO)_9(\mu_3\text{-}Se)_2]$ (**1Se**), the latter being studied in order to compare with previous studies of $[Fe_3(CO)_9(\mu_3\text{-}S)_2]$ (**1S**) [14,15].

2. Experimental

2.1. General procedures

Unless otherwise stated, purification of solvents, reactions, and manipulation of compounds were carried out under a nitrogen atmosphere using standard Schlenk techniques. Reagent grade solvents were dried by standard procedures and were freshly distilled prior to use. All chromatographic separations and ensuing workup were carried out in air. Thin layer chromatography was carried out on glass plates pre-coated with Merck 60 0.25 mm silica gel. Dppm was purchased from Acros Organics Chemicals Inc. and $[Fe_3(CO)_{12}]$, $[Fe(CO)_5]$, elemental sulfur and selenium were purchased from Sigma-Aldrich; $[Fe_3(CO)_{10}(\mu\text{-dppm})]$ [28] and $[Fe_3(CO)_9(\mu_3\text{-}S)_2]$ (**1S**) [29] were prepared as previously reported. Infrared spectra were recorded on Nicolet 6700 FT-IR or Nicolet Avatar 360 FT-IR-spectrometers in a solution cell fitted with CaF_2 or NaCl plates, subtraction of the solvent absorptions being achieved by computation. Fast atom bombardment (FAB) mass spectra were obtained on a JEOL SX-102 spectrometer using 3-nitrobenzyl alcohol as matrix and CsI as calibrant. Proton and $^{31}P\{^1H\}$ NMR spectra were recorded on Varian Unity 500 MHz or Bruker AMX400 instruments. Chemical shifts were referenced to residual solvent or 85% H_3PO_4. Elemental analyses were performed at University College London.

2.2. Synthesis of $[Fe_3(CO)_9(\mu_3\text{-}Se)_2]$ (**1Se**) [30]

A benzene solution (20 mL) of $[Fe_3(CO)_{12}]$ (100 mg, 0.198 mmol) and selenium (31 mg, 0.398 mmol) was refluxed for 20 h. The solvent was removed under reduced pressure, and the solvent was removed *in vacuo* and the residue extracted with hexane and filtered on Kieselguhr. The faster moving band gave $[Fe_3(CO)_9(\mu_3\text{-}Se)_2]$ (**1Se**) (20 mg, 17%) [30] (IR (ν(CO), n-hexane): 2071w, 2056vs, 2037vs, 2017s, 2002br, 1982sh cm^{-1}) as black crystals after recrystallization from hexane/CH_2Cl_2 at 4 °C.

2.3. Synthesis of $[Fe_3(CO)_7(\mu_3\text{-}CO)(\mu_3\text{-}S)(\mu\text{-dppm})]$ (**2S**) and $[Fe_3(CO)_7(\mu_3\text{-}S)_2(\mu\text{-dppm})]$ (**3S**)

A number of routes were used to access these clusters. (i) A CH_2Cl_2 solution (20 mL) of $[Fe_3(CO)_{10}(\mu\text{-dppm})]$ (40 mg, 0.048 mmol) and sulfur (3.1 mg, 0.096 mmol) was refluxed for 10 h. The solvent was removed under reduced pressure, and the residue was chromatographed by TLC on silica gel. Elution with cyclohexane/CH_2Cl_2 (9:1 v/v) developed three bands. The faster moving band gave $[Fe_3(CO)_7(\mu_3\text{-}S)_2(\mu\text{-dppm})]$ (**3S**) (6 mg, 15%), the second band was unreacted $[Fe_3(CO)_{10}(\mu\text{-dppm})]$ (2 mg) and the third afforded $[Fe_3(CO)_7(\mu_3\text{-}CO)(\mu_3\text{-}S)(\mu\text{-dppm})]$ (**2S**) (20 mg, 51%) as red crystals after recrystallization from hexane/CH_2Cl_2 at 4 °C. (ii) A benzene solution (20 mL) of $[Fe_3(CO)_9(\mu_3\text{-}S)_2]$ (**1S**) (18 mg, 0.037 mmol) and dppm (15 mg, 0.037 mmol) was refluxed for 30 min. Solvent was removed under reduced pressure, and the residue was chromatographed by TLC on silica gel. Elution with cyclohexane/CH_2Cl_2 (3:1 v/v) developed three bands. The faster moving band was unreacted $[Fe_3(CO)_9(\mu_3\text{-}S)_2]$ (**1S**) (2.0 mg), the second band afforded $[Fe_3(CO)_7(\mu_3\text{-}S)_2(\mu\text{-dppm})]$ (**3S**) (6.0 mg, 20%) and the third band afforded $[Fe_3(CO)_7(\mu_3\text{-}CO)(\mu_3\text{-}S)(\mu\text{-dppm})]$ (**2S**) (9.0 mg, 33%). (iii) A CH_2Cl_2 solution (20 mL) of $[Fe_3(CO)_7(\mu_3\text{-}CO)(\mu_3\text{-}S)(\mu\text{-dppm})]$ (**2S**) (20 mg, 0.025 mmol) and sulfur (1.6 mg, 0.049 mmol) was refluxed for 1 day. The solvent was removed under reduced pressure, and the residue was chromatographed by TLC on silica gel. Elution with cyclohexane/CH_2Cl_2 (9:1 v/v) developed two bands. The faster moving band gave **3S** (3.0 mg, 14%), the second band was unreacted **2S** (10 mg). (iv) A benzene solution (20 mL) of **1S** (18 mg, 0.037 mmol) and dppm (15 mg, 0.037 mmol) was refluxed for 30 min. The solvent was removed under reduced pressure, and the residue was chromatographed by TLC on silica gel. Elution with cyclohexane/CH_2Cl_2 (3:1 v/v) developed two bands. The faster moving band was unreacted **1S** (2.0 mg) and the second band afforded **3S** (8 mg, 34%). Characterising data. **2S**: Anal. Calcd for $C_{33}H_{22}Fe_3O_8SP_2$: C, 49.97; H, 2.72 Found: C, 49.1; H, 2.78. IR (ν(CO), CH_2Cl_2): 2057s, 2006vs, 1962sh, 1666w cm^{-1}. ^1H NMR ($CDCl_3$): δ 7.6–7.1 (m, 20 H), 3.45 (m, br), 2 H, CH_2). $^{31}P\{^1H\}$ NMR ($CDCl_3$): δ 55.4 (s). ESI-MS: *m/z* 808 .10 found, *m/z* 807.85 calc for $[M^+]$. **3S**: Anal. Calcd for $C_{32}H_{22}Fe_3O_7S_2P_2$: C, 47.29; H, 2.70 Found: C, 47.50; H, 2.71. IR (ν(CO), CH_2Cl_2): 2045s, 2000vs, 1961w, 1930br cm^{-1}. ^1H NMR ($CDCl_3$): δ 7.75-7.33 (m, 20H), 2.98 (t, 2H, J 10 Hz). $^{31}P\{^1H\}$ NMR ($CDCl_3$): δ 75.3 (s).

2.4. Synthesis of $[Fe_3(CO)_7(\mu_3\text{-}CO)(\mu_3\text{-}Se)(\mu\text{-dppm})]$ (**2Se**) and $[Fe_3(CO)_7(\mu_3\text{-}Se)_2(\mu\text{-dppm})]$ (**3Se**)

A number of routes were used to access these clusters. (i) A CH_2Cl_2 solution (20 mL) of $[Fe_3(CO)_{10}(\mu\text{-dppm})]$ (30 mg, 0.036 mmol) and selenium (6.0 mg, 0.071 mmol) was refluxed for 10 h. The solvent was removed under reduced pressure, and the residue was chromatographed by TLC on silica gel. Elution with cyclohexane/CH_2Cl_2 (9:1 v/v) developed three bands. The faster moving band gave $[Fe_3(CO)_7(\mu_3\text{-}Se)_2(\mu\text{-dppm})]$ (**3Se**) (7.0 mg, 21%), the second band was unreacted $[Fe_3(CO)_{10}(\mu\text{-dppm})]$ (1 mg) and the third afforded $[Fe_3(CO)_7(\mu_3\text{-}CO)(\mu_3\text{-}Se)(\mu\text{-dppm})]$ (**2Se**) (17 mg, 55%) as red crystals after recrystallization from hexane/CH_2Cl_2 at 4 °C. (ii) A CH_2Cl_2 solution (20 mL) of $[Fe_3(CO)_7(\mu_3\text{-}CO)(\mu_3\text{-}Se)(\mu\text{-dppm})]$ (**2Se**) (20 mg, 0.023 mmol) and selenium (4.0 mg, 0.047 mmol) was refluxed for 1 day. The solvent was removed under reduced pressure, and the residue was chromatographed by

TLC on silica gel. Elution with cyclohexane/CH_2Cl_2 (9:1 v/v) developed two bands. The faster moving band gave [$Fe_3(CO)_7(\mu_3$-Se$)_2(\mu$-dppm)] (**3Se**) (4.0 mg, 19%), the second band was unreacted [$Fe_3(CO)_7(\mu_3$-CO$)(\mu_3$-Se$)(\mu$-dppm)] (**2Se**) (9.0 mg). (iii) A benzene solution (20 mL) of **1Se** (25 mg, 0.0432 mmol) and dppm (18 mg, 0.0432 mmol) was refluxed for 2 h. The solvent was removed under reduced pressure, and the residue was chromatographed by TLC on silica gel. Elution with cyclohexane/CH_2Cl_2 (7:3 v/v) developed two bands. The faster moving band was unreacted **1Se** (5.0 mg) and the second band afforded **3Se** (6.0 mg, 19%). Characterising data. **2Se**: Anal. Calcd for $C_{33}H_{22}Fe_3O_8SeP_2$: C, 46.31; H, 2.57. Found: C, 46.35; H, 2.60. IR (ν(CO), CH_2Cl_2): 2053s, 2003vs, 1957sh, 1659 cm^{-1}. ^1H NMR ($CDCl_3$): δ 7.55-7.38 (m, 15 H), 7.23-7.13 (m, 5 H), 3.68 (br, 1 H, CH_2), 3.47 (br, 1H, CH_2). $^{31}P\{^1H\}$ NMR ($CDCl_3$): δ 55.3 (s). ESI-MS: *m/z* 855.12 found, *m/z* 855.80 calc for [M^+]. **3Se**: Anal. Calcd for $C_{32}H_{22}Fe_3O_7Se_2P_2$: C, 42.38; H, 2.42 Found: C, 42.75; H, 2.55. IR (ν(CO), CH_2Cl_2): 2050s, 2040s, 1991vs, 1942w cm^{-1}. ^1H NMR ($CDCl_3$): δ 7.89 (m, 1H), 7.76 (br, 2H), 7.65 (m, 4H), 7.52 (t, 2H, J 10 Hz), 7.38 - 7.33 (m, 11H), 4.02 (br, 2H, CH_2, **B**), 3.16 (t, 2H, CH_2, J 10 Hz, **A**). $^{31}P\{^1H\}$ NMR ($CDCl_3$): δ 78.7 (s, **B**), 53.0 (d, **A**), 42.6 (d, **A**) J_{PP} 56 Hz,. Ratio **A**:**B** *ca.* 2:3 (see text).

2.5. Protonation experiments

To CH_2Cl_2 solutions (*ca.* 1 mL) of the triiron clusters (made by dissolving 1×10^{-3} mmol of each complex) were added 2 molar equivalents of $HBF_4 \cdot Et_2O$. The resultant acid-containing solution was immediately transferred to an IR cell and monitored over time.

2.6. X-ray structure determinations

Crystals of **2S**, **2Se**, **3S** and **3Se** suitable for X-ray structure analysis were grown by slow diffusion of hexane into a saturated CH_2Cl_2 solution at 4 °C. Crystals were immersed in cryo-oil, mounted on a Nylon loop, and measured at a temperature of 120–170 K. The X-ray diffraction data were collected on a Bruker Kappa Apex II Duo or an Agilent Supernova diffractometer using Mo Kα radiation ($\lambda = 0.71073$ Å). The APEX2 [31] or CrysAlisPro [32] program packages were used for cell refinements and data reductions. Structures were solved by direct methods or by charge flipping using the SHELXS-97 [33] or SUPERFLIP [34] programs. A multi-scan, numerical, or Gaussian absorption correction (SADABS [35] or CrysAlisPro [32]) was applied to all data. Structural refinements were carried out using SHELXL-97 or SHELXL-2013 [33]. The hydrogen atoms were positioned geometrically and constrained to ride on their parent atoms, with C-H = 0.95–0.99 Å and $U_{iso} = 1.2\ U_{eq}$ (parent atom). Crystallographic details are summarised in Table S1.

2.7. Electrochemistry

Electrochemistry was carried out under solvent-saturated nitrogen in deoxygenated MeCN and CH_2Cl_2 solutions with 0.1 M [NBu_4][PF_6] as the supporting electrolyte. The working electrode was a 3 mm diameter glassy carbon electrode that was polished with 0.3 μm alumina slurry as needed, the counter electrode was a platinum wire, and the reference electrode was either a silver wire or an Ag/AgCl electrode that was separated from the working electrode by a glass frit. Potentials are referenced versus the ferrocenium/ferrocene couple (Fc^+/Fc). A Pine potentiostat (Pine WaveNow potentiostat) was used for all electrochemical measurements. Catalysis studies were carried out by adding equivalents of *p*-TsOH and $HBF_4 \cdot Et_2O$ (Sigma-Aldrich).

2.8. Computational details and modelling

All DFT calculations were carried out with the Gaussian 09 package of programs [36] using the B3LYP hybrid functional. This functional is comprised of Becke's three-parameter hybrid exchange functional (B3) [37] and the correlation functional of Lee, Yang, and Parr (LYP) [38]. Each iron atom was described with the Stuttgart-Dresden effective core potential and SDD basis set [39] and the 6-31G(d') basis set [40] was employed for all remaining atoms. All reported geometries were fully optimized, and analytical second derivatives confirmed each structure as an energy minimum (no negative eigenvalues). Unscaled vibrational frequencies were used to make zero-point and thermal corrections to the electronic energies, and the resulting free energies are reported in kcal mol^{-1} relative to the specified standard. The reported carbonyl stretching bands for species **C** (vide infra, Section 3.3) were obtained from the harmonic frequencies and have been scaled using a factor of 0.965. The Natural Population Analysis (NPA) and Wiberg bond indices (WBI) were computed using Weinhold's natural bond orbital (NBO) program, as executed by Gaussian 09 [41,42]. The geometry-optimized structures have been drawn with the *JIMP2* molecular visualization and manipulation program [43].

3. Results and discussion

3.1. Synthesis and characterisation

For [$Fe_3(CO)_7(\mu_3$-CO$)(\mu_3$-E$)(\mu$-dppm)] (**2**) (E = S, Se) two pathways were considered; (i) addition of dppm to [$Fe_3(CO)_9(\mu_3$-CO$)(\mu_3$-E)] (**1**) [44,45] and (ii) addition of group 16 elements to [$Fe_3(CO)_{10}(\mu$-dppm)] [28]. Sulfide-capped [$Fe_3(CO)_9(\mu_3$-CO$)(\mu_3$-S)] has previously been reported [41] but yields were low and separation (from other sulfur-containing species) difficult. A brief report of [$Fe_3(CO)_9(\mu_3$-CO$)(\mu_3$-Se)] has appeared; it was formed in low yield upon addition of $BiCl_3$ to K_2[$Fe_3(CO)_9(\mu_3$-Se)] [45]. In line with the established increase in stabilisation of the triruthenium centre in [$Ru_3(CO)_{10}(\mu$-dppm)] [46] as compared to [$Ru_3(CO)_{12}$], it was expected that the triiron core of [$Fe_3(CO)_{10}(\mu$-dppm)] [28] will be less susceptible to fragmentation than that of [$Fe_3(CO)_{12}$]. This was found to be the case and the isostructural clusters, [$Fe_3(CO)_7(\mu_3$-CO$)(\mu_3$-E$)(\mu$-dppm)] (E = S, Se) (**2**), were prepared in moderate yields upon heating CH_2Cl_2 solutions of [$Fe_3(CO)_{10}(\mu$-dppm)] with elemental sulfur or selenium. Minor products were known bis(-chalcogenide) clusters [$Fe_3(CO)_7(\mu_3$-E$)_2(\mu$-dppm)] (**3**) [47,48] (Scheme 1), previously prepared by addition of $dppmS_2$ [17] or

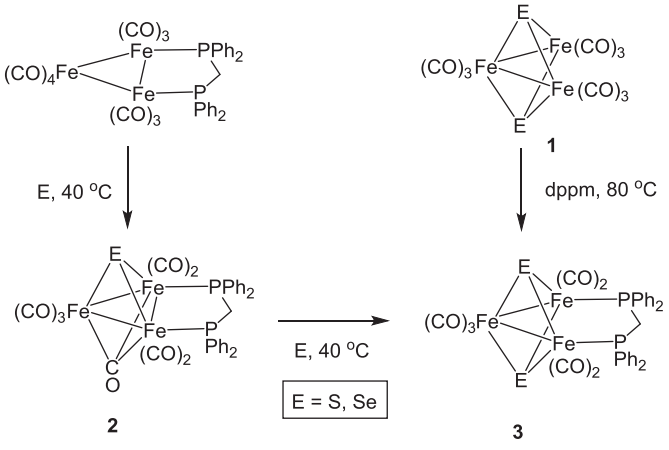

Scheme 1. Synthesis of chalcogenide-capped clusters **2-3**.

dppmSe$_2$ [48] to [Fe$_3$(CO)$_{12}$]. In separate experiments **2S** and **2Se** reacted with excess chalcogenide over 10 h to afford **3S** and **3Se**, respectively, indicating that chalcogenide-capping takes place in a stepwise fashion. While **1Se** is known [30], we have found that it may be prepared in a single step from elemental selenium and [Fe$_3$(CO)$_{12}$]. Reactions of **1S** and **1Se** with dppm in refluxing CH_2Cl_2 afford **3S** and **3Se**, respectively, in moderate yields.

3.2. Structural studies

Molecular structures of [Fe$_3$(CO)$_7$(μ$_3$-CO)(μ$_3$-S)(μ-dppm)] (**2S**) and [Fe$_3$(CO)$_7$(μ$_3$-CO)(μ$_3$-Se)(μ-dppm)] (**2Se**) are depicted in Fig. 1. Those of [Fe$_3$(CO)$_7$(μ$_3$-S)$_2$(μ-dppm)] (**3S**) [17] and [Fe$_3$(CO)$_7$(μ$_3$-Se)$_2$(μ-dppm)] (**3Se**) [48] have been previously reported but for comparison we have also collected data (see ESI). Important metric parameters are summarised in Table S1 and selected bond lengths and angles in Table S2.

Spectroscopic data for **2** are consistent with the solid-state structure being maintained in solution. IR spectra contain an absorption between 1650 and 1670 cm^{-1}, confirming the presence of the triply-bridging carbonyl. Each displays well-resolved ^{1}H and ^{31}P{^{1}H} NMR spectra, the latter consisting of a singlet at *ca.* 55.5 ppm for the two equivalent phosphorus atoms. For **3** in the solid-state the diphosphine spans the non-bonded iron-iron edge, but NMR spectroscopy indicates that in solution **3Se** exists as a mixture of isomers. This is most clearly seen in the ^{31}P{^{1}H} NMR spectrum which consists of a pair of doublets and a singlet that are attributed to isomer **A** and **B** (Chart 1) respectively (*cf.* Experimental Section). All resonances are well-resolved, showing that interconversion of the isomers is slow on the NMR time scale.

3.3. Reactions with Brönsted and Lewis acids

Protonation of the metal core is a key feature of proton-reduction catalysis; we thus investigated the behaviour of these clusters towards strong acids. The addition of 2-3 equivalents of $HBF_4{\cdot}Et_2O$ to CH_2Cl_2 solutions of [Fe$_3$(CO)$_9$(μ$_3$-Se)$_2$] (**1Se**) did not result in any significant changes in the IR spectrum consistent with the triiron centre not being sufficiently basic to be protonated under these conditions. Addition of two equivalents of $HBF_4{\cdot}Et_2O$ to [Fe$_3$(CO)$_7$(μ$_3$-CO)(μ$_3$-S)(μ-dppm)] (**2S**) and [Fe$_3$(CO)$_7$(μ$_3$-CO)(μ$_3$-Se)(μ-dppm)] (**2Se**) led to an immediate change in both cases with all bands being shifted to higher wavenumbers by *ca.* 20-30 cm^{-1} (Scheme 2). Thus, absorptions at 2057, 2006, 1962 and 1666 cm^{-1} for **2S** were replaced by new peaks at 2086, 2047, 2029 and 2008 cm^{-1}. The magnitude of this change suggests no significant change in electron-density at the triiron centre; metal-centred protonation is expected to result in a ~50-70 cm^{-1} positive shift [49]. The relatively symmetric IR spectrum suggests a reaction site at one of the face-capping ligands, with the μ$_3$-CO group being implicated on the basis of the absence of the face-capping ν(CO) band. Monitoring reactions of **2** with $HBF_4{\cdot}Et_2O$ (in $CDCl_3$) by ^{1}H NMR spectroscopy revealed no evidence of hydride formation. Noting that HBF_4 is a complex of BF_3 and HF, we added $BF_3{\cdot}Et_2O$ to CH_2Cl_2 solutions of both **2S** and **2Se** and observed IR spectra identical to those generated upon addition of $HBF_4{\cdot}Et_2O$. Addition of piperidine led to regeneration of the starting clusters, indicating that the so-called "protonation reaction" simply reflects the reversible addition of BF_3 to the face-capping μ$_3$-CO ligand (Scheme 2).

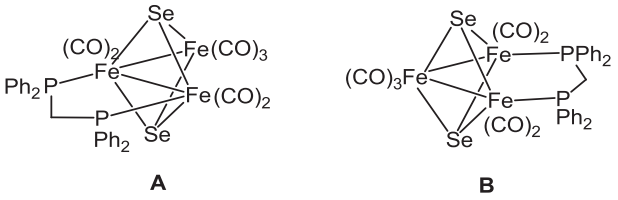

Chart 1. Two isomers of **3Se**.

We thus conclude that addition of both $HBF_4{\cdot}Et_2O$ to **2** leads to formation of [Fe$_3$(CO)$_7$(μ$_3$-COBF$_3$)(μ$_3$-E)(μ-dppm)] (**2.BF$_3$**). This was investigated by DFT calculations employing optimized structures of **2S** (species **A**) and BF_3 (both of which are not shown) for the ensuing stability calculations. Interestingly, coordination of the chalcogenide in **A** by BF_3 does not afford a stable species, this adduct spontaneously liberating **2S** and free BF_3. A stable BF_3 complex is, however, obtained when the oxygen atom of the μ$_3$-CO ligand functions as a Lewis base, and the geometry-optimized structure of this adduct (species **B**) is depicted in Fig. S1. Table S3 summarises the natural charges and Wiberg bond indices for **A** and **B**, and the data confirm that the coordinated BF_3 molecule in **B** does not adversely perturb the charges or bond orders within the Fe$_3$ core relative to the parent cluster **A**. Scaled frequencies of the major ν(CO) bands in **B** are 2074, 2041, 2028, and 1998 cm^{-1}, in good agreement with IR solution data. This led us to discard

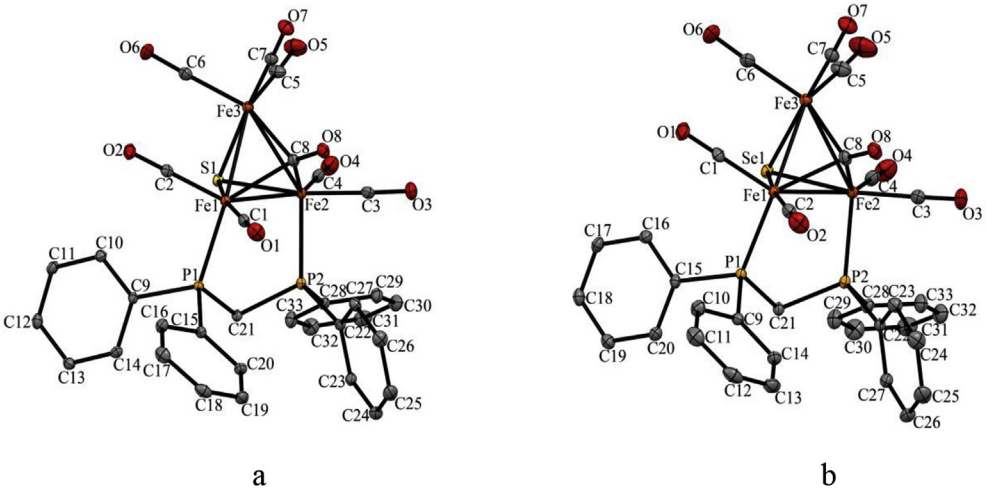

Fig. 1. Molecular structures of (a) [Fe$_3$(CO)$_7$(μ$_3$-CO)(μ$_3$-S)(μ-dppm)] (**2S**) and (b) [Fe$_3$(CO)$_7$(μ$_3$-CO)(μ$_3$-Se)(μ-dppm)] (**2Se**).

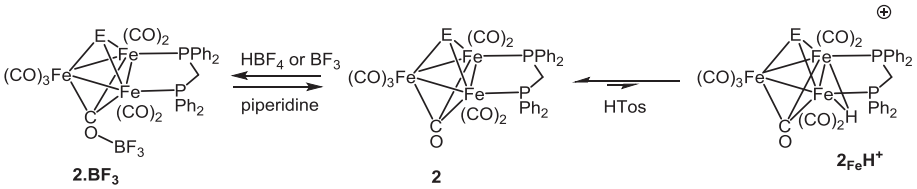

Scheme 2. Proposed interaction of Lewis and Brönstead acids with **2**.

$HBF_4 \cdot Et_2O$ as a proton source for catalytic studies. Addition of two equivalents of *p*-TsOH to a CH_2Cl_2 solution of **2S** did not lead to major changes in the IR spectrum; a small (<5%) new absorption appeared at 2085 cm^{-1}, the intensity of which did not change with time. We, therefore, elected to use this acid for electrocatalytic proton-reduction studies (*vide infra*).

We also probed reactions of **3** with two equivalents of $HBF_4 \cdot Et_2O$. For **3S**, peaks at 2045s, 2000vs, 1961w, 1930br cm^{-1} were very slowly (over 24 h) replaced by new absorptions at 2102 m, 2065sh, 2046s and 2004 m cm^{-1} which we associate with $[Fe_3(CO)_7(\mu\text{-}H)(\mu_3\text{-}S)_2(\mu\text{-dppm})][BF_4]$ (**3SH**$^+$), while for **3Se** the analogous species is associated with peaks at 2097 m, 2055w,sh, 2039vs and 1996 m cm^{-1}, being generated at a similar rate (Scheme 3). Attempts to observe hydride species by NMR spectroscopy were unsuccessful in both cases. We also protonated **3S** with 2 equivalents of *p*-TsOH and again there was some evidence of formation of small amounts of **3SH**$^+$ after 3 h (ca. 10% as estimated by band intensity). Kaiser and Knör have published details of a protonation study of **3S** by CF_3CO_2H and provide evidence from differential IR spectroscopy of both mono- and di-protonated complexes of **3S** [17]. The latter is apparently characterised by an absorption at 2144 cm^{-1}, but we have not been able to observe any absorption in this region. It seems likely that our results differ from those of Kaiser and Knör as a result of the different concentrations of acids added and the quality of IR equipment used. What is clear is that protonation of **3S** and **3Se** is slow (especially when compared to the time scale for the cyclic voltammetry experiments), and thus, while **3H**$^+$ are chemically accessible, we conclude that they are not catalytically relevant.

In order to better understand the reactivity of clusters **2S** and **3S** in the presence of strong acids, we carried out DFT calculations on the preferred sites of protonation. Optimized structures for $[Fe_3(CO)_7(\mu_3\text{-}CO)(\mu_3\text{-}S)(\mu\text{-dppm})]$ (**A**) and $[Fe_3(CO)_7(\mu_3\text{-}S)_2(\mu\text{-dppm})]$ (**D**) are in accord with reported solid-state structures. The DFT data indicate that the preferred site of protonation in **A** coincides with the dppm-substituted iron-iron vector to give **2$_{Fe}$H**$^+$ (species **C1**), as depicted in Scheme 2. The HOMO in **A** (not shown) is a metal-based orbital whose parentage is not unlike that computed earlier by Schilling and Hoffmann in related tetrahedral clusters [50], with the largest concentration of electron density located between the iron centres ligated by the dppm ligand. Fig. 2 shows the geometry-optimized structure of the thermodynamically favoured product **C1**. Protonation of the non-dppm ligated metal-metal bond in **A** affords **C2**, which is 3.8 kcal mol^{-1} less stable than **C1**. Protonation of the oxygen and sulfur sites associated with the μ_3-CO and μ_3-S moieties furnishes species **C3** and **C4**, respectively. In comparison with the **C1** and **C2** hydride species, these latter two species are not energetically favoured in the protonation of **A**. Protonation of the μ_3-S group is the least stable of the protonated species computed, lying 30.5 kcal mol^{-1} above **A**.

The protonation of the iron-iron bond in **C1** and **C2** leads to slight changes in the charge at the iron centres but more significant are the structural changes in the face-capping carbonyl group. Protonation is accompanied by lengthening of two of the three Fe-μ_3-CO bonds to afford a pseudo-terminal CO ligand. The slippage of the μ_3-CO ligand in both **C1** and **C2** is visually verified in the optimized structures, and this feature is reflected by the Wiberg bond indices that reveal a CO group that is asymmetrically bound to the three iron atoms. In the case of **C1**, the computed Wiberg bond indices for the original face-capping CO group are 0.33 (Fe_1-CO), 0.16 (Fe_2-CO), and 0.93 (Fe_3-CO). These indices suggest that this particular CO group is best viewed as a pseudo-terminal ligand at Fe_3 and that this particular CO exhibits semi-bridging interactions with the Fe_1 and Fe_2 centres. **C2** displays similar behaviour for the face-capping CO upon protonation, and here the Fe_1 centre serves as the site of coordination for the pseudo-terminal CO ligand. The Wiberg bond indices of 0.46 and 0.19 for the Fe_2-CO and Fe_3-CO vectors in **C2** underscore this assertion.

The site of protonation in **3S** was also examined by DFT. Cluster **3S** was optimized (species **D**, not shown) and subsequently employed in the protonation studies. Fig. 3 shows the optimized structures and energy ordering for **E1** and **E2**, which correspond to the products from Fe-Fe bond and sulfur protonation, respectively. Protonation of the Fe-Fe bond in **D** is clearly favoured over protonation of one of the face-capping sulfide ligands. The computed HOMO in **D** (not shown) is best described as a metal-based bonding orbital where the electron density is localized about the two formal Fe-Fe bonds in the *nido* polyhedral core. Examination of the Wiberg bond indices for the Fe_1-Fe_3 (0.30) and Fe_2-Fe_3 (0.18) bonds in **E1** provides insight into the structural changes that occur upon protonation. The Wiberg bond index for the protonation of an Fe-Fe

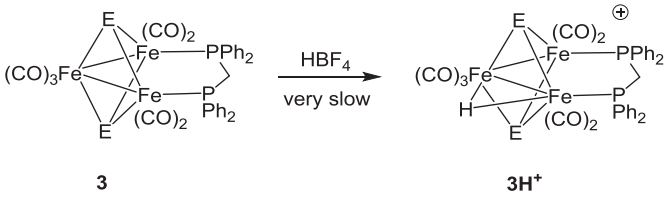

Scheme 3. Protonation of **3**.

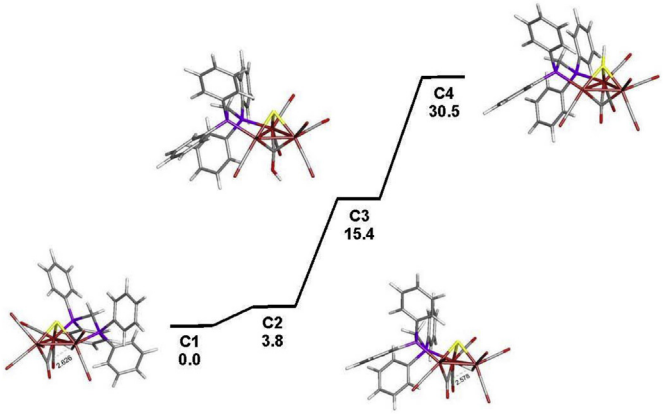

Fig. 2. Ground-state energy ordering of the different protonated species (**C1**-**C4**) from $[Fe_3(CO)_7(\mu_3\text{-}CO)(\mu_3\text{-}S)(dppm)]$ (**A**). Energy values (ΔG) are in kcal mol^{-1} relative to **C1**.

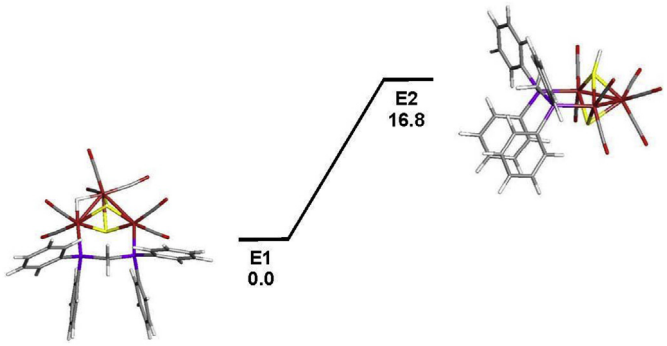

Fig. 3. Ground-state energy ordering for the different protonated species **E1** and **E2** from $[Fe_3(CO)_7(\mu_3\text{-}S)_2(dppm)]$ (**D**). Energy values (ΔG) are in kcal mol^{-1} relative to **E1**.

bond changes little relative to the parent cluster **D**, whose mean index for the pairwise equivalent Fe-Fe bonds is 0.35. The non-bonding $Fe_1\cdots Fe_2$ centres in species **D**, **E1**, and **E2** all display negligible Wiberg bond indices consistent with the absence of a significant orbital overlap between these metal centres. In response to protonation of the Fe_1-Fe_3 bond in **E1**, the Fe_2-Fe_3 bond undergoes an elongation (ca. 0.18 Å relative to the mean 2.636 Å bond distance computed for the Fe-Fe bonds in **D**) and a weakening of the metal-metal bond.

3.4. Electrochemical studies

The sulfide cluster $[Fe_3(CO)_9(\mu_3\text{-}S)_2]$ (**1S**) is reported to undergo two one-electron reduction processes at -0.94 V (reversible) and -1.75 V (irreversible) in MeCN and an irreversible oxidation was also observed at +0.80 V [14]. In MeCN, $[Fe_3(CO)_9(\mu_3\text{-}Se)_2]$ (**1Se**) (Fig. 4) also shows three reduction waves; at $E_{1/2} = -0.96$ V (reversible, $\Delta E = 70$ mV), -1.70 V (quasi-reversible) and −2.5 V (irreversible) and an irreversible oxidation at $E_p = +0.80$ V. Reversibility of the second reduction wave improves at higher scan rates (≥0.025 Vs^{-1}), this quasi-reversibility being the main difference in the electrochemical behaviour of **1S** and **1Se**.

Mono-capped $[Fe_3(CO)_7(\mu_3\text{-}CO)(\mu_3\text{-}S)(\mu\text{-}dppm)]$ (**2S**) and $[Fe_3(CO)_7(\mu_3\text{-}CO)(\mu_3\text{-}Se)(\mu\text{-}dppm)]$ (**2Se**) were also studied in MeCN (Fig. S3) and for comparison with **1** and in CH_2Cl_2 (Fig. 5 and Fig. S2) as proton-reduction catalysis was carried out in this solvent (*vide infra*). In CH_2Cl_2, **2S** and **2Se** display similar reductive behaviour, showing a quasi-reversible reduction at $E_{1/2} = -1.29$ V ($\Delta E = 230$ mV) for **2S** and at $E_{1/2} = -1.30$ V ($\Delta E = 308$ mV) for **2Se**. A second peak is seen for both on the return scan (E_p = -0.58 for **2S** and -0.64 V for **2Se**), but this was not further investigated. The two clusters display somewhat different oxidation behaviour, but for both all oxidative processes are irreversible. For **2S** a single oxidation process is seen at +0.81 V, while for **2Se** two separate oxidation waves are seen at +0.55 and + 1.00 V. As the first oxidation wave for **2S** occurs at more positive potential than for **2Se**, we deem it likely that a second oxidation wave for **2S** is out of the solvent window. In MeCN, the first reduction of each cluster occurs at lower potentials than in CH_2Cl_2 and becomes reversible; for **2S** $E_{1/2} = -1.16$ V ($\Delta E = 80$ mV) for **2Se** $E_{1/2} = -1.15$ V ($\Delta E = 90$ mV), and the small additional oxidation on the reverse scan remains. For **2S** an irreversible oxidation feature is again observed (at +0.20 V). Oxidation of **2Se** is complicated, the main oxidation at +0.28 V being followed by poorly defined further oxidative features, all irreversible. The electrochemical behaviour of **2S** contrasts with that reported for $[Fe_3(CO)_9(\mu_3\text{-}CO)(\mu_3\text{-}S)]$ [51], where both reduction and oxidation (at -0.26 and + 0.43 V respectively) are irreversible. Thus, coordination of the diphosphine stabilises the reduced product while shifting it more negative by *ca.* 1 V.

CVs of $[Fe_3(CO)_7(\mu_3\text{-}S)_2(\mu\text{-}dppm)]$ (**3S**) and $[Fe_3(CO)_7(\mu_3\text{-}Se)_2(\mu\text{-}dppm)]$ (**3Se**) were carried out in CH_2Cl_2 (Fig. 6) and MeCN (Fig. S4). In CH_2Cl_2, **3S** displays a quasi-reversible reduction ($E_{1/2}$ = -1.55 V, ΔE = 215 mV) together with two oxidation waves at +0.36 and + 0.57 V. The second is almost completely irreversible, but the first has a small degree of quasi-reversibility ($\Delta E = 205$ mV). The selenium analogue **3Se** shows two reduction waves within the potential window of CH_2Cl_2, the first reduction is reversible and appearing at ca. 0.1 V lower potential ($E_{1/2}$ = -1.45 V, $\Delta E = 81$ mV) and a second irreversible reduction appears at -2.13 V. The oxidation behaviour with **3Se** is very similar to that of **3S**, showing two processes at +0.38 and + 0.63 V, the second being completely irreversible, while the first has a hint of quasi-reversibility ($\Delta E = 174$ mV). When the scan rate was varied between 0.01 and 0.50 V^{-1} for **3S** and 0.025-2.0 V^{-1} for **3Se**, no additional features were observed (Fig. S4). In MeCN, slightly different behaviour is noted for both clusters (Fig. S5). Most notably a second reduction

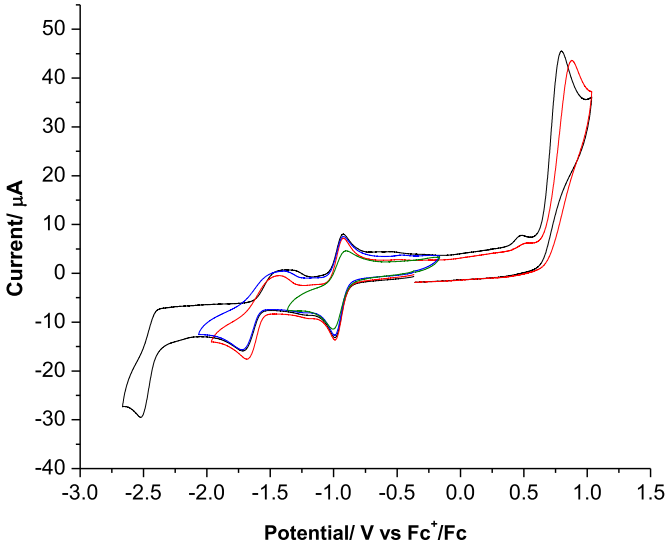

Fig. 4. CVs of $[Fe_3(CO)_9(\mu_3\text{-}Se)_2]$ (**1Se**) in MeCN (1 mM solution, supporting electrolyte $[NBu_4][PF_6]$, scan rate 0.1 V^{-1}, glassy carbon electrode, potential vs Fc^+/Fc).

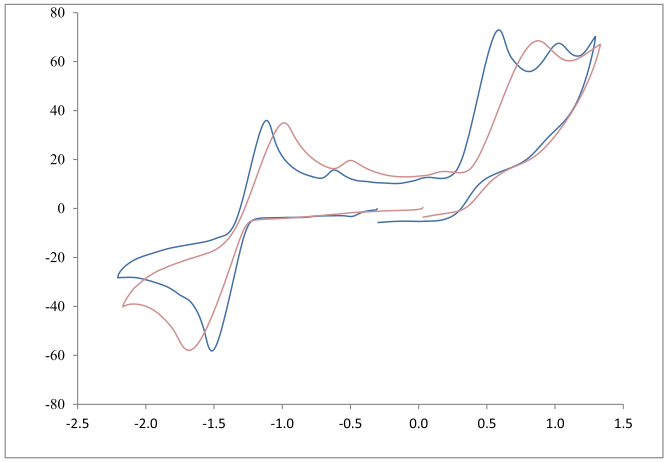

Fig. 5. CVs of (a) $[Fe_3(CO)_7(\mu_3\text{-}CO)(\mu_3\text{-}S)(\mu\text{-}dppm)]$ (**2S**) (red) and (b) $[Fe_3(CO)_7(\mu_3\text{-}CO)(\mu_3\text{-}Se)(\mu\text{-}dppm)]$ (**2Se**) (blue) in CH_2Cl_2 (1 mM solution, supporting electrolyte $[NBu_4][PF_6]$, scan rate 0.250Vs^{-1} glassy carbon electrode, potential vs Fc^+/Fc). (For interpretation of the references to colour in this figure legend, the reader is referred to the Web version of this article.)

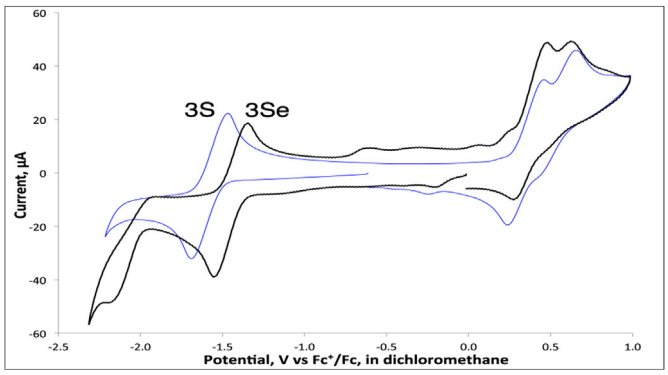

Fig. 6. CVs of $[Fe_3(CO)_7(\mu_3\text{-}S)_2(\mu\text{-}dppm)]$ (**3S**) (blue) and $[Fe_3(CO)_7(\mu_3\text{-}Se)_2(\mu\text{-}dppm)]$ (**3Se**) (black) in CH_2Cl_2 (1 mM solution, supporting electrolyte $[NBu_4][PF_6]$, scan rate 0.25 V^{-1}, glassy carbon electrode, potential vs Fc^+/Fc). (For interpretation of the references to colour in this figure legend, the reader is referred to the Web version of this article.)

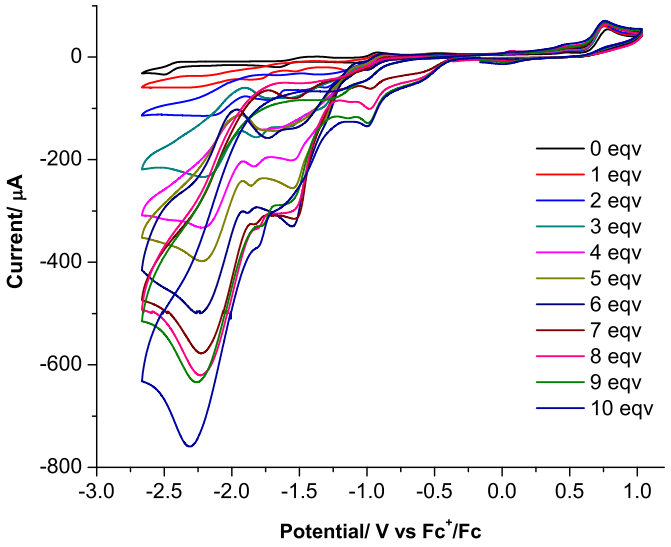

Fig. 7. CVs of **1Se** in MeCN in the absence and presence of 1–10 molar equivalents of $HBF_4{\cdot}Et_2O$ (1 mM solution, supporting electrolyte $[NBu_4][PF_6]$, scan rate 0.1 $V\,s^{-1}$, glassy carbon electrode, potential vs. Fc^+/Fc).

process is seen for **3S**, and the second reduction of **3Se** that appears at -1.94 V becomes quasi-reversible. Thus, it is clear that the cluster anions are stabilised in MeCN with respect to CH_2Cl_2. Both clusters now show a single irreversible oxidation wave at +0.36 and + 0.45 V for **3Se** and **3S**, respectively. In summary, for all three cluster types oxidation occurs at relatively low potentials but is irreversible. The first reduction is reversible or quasi-reversible, suggesting that the radical anions have some stability, which bears well for their proposed proton-reduction chemistry. Redox potentials are not particularly sensitive to the nature of the chalcogenide and, as expected, the introduction of the diphosphine results in a shift of oxidation potentials to less positive and reduction potentials to more negative values.

3.5. Electrocatalytic studies

With weak acids $[Fe_3(CO)_9(\mu_3\text{-}S)_2]$ (**1S**) [14] is catalytically active only at the second reduction potential, but with strong acids, it is catalytic at both the first and second reduction potential [15]. We studied the catalytic proton-reduction behaviour of $[Fe_3(CO)_9(\mu_3\text{-}Se)_2]$ (**1Se**) in both CH_2Cl_2 (Fig. S6) and MeCN (Fig. 7) but only discuss the latter as it allows a direct comparison with **1S**. IR studies (*vide supra*) showed that **1Se** does not protonate upon addition of $HBF_4{\cdot}Et_2O$ and thus the first step in any catalytic proton-reduction is reduction. On addition of one to ten molar equivalent of $HBF_4{\cdot}Et_2O$ to **1Se**, a series of complex CVs result with up to five successive peaks being observed in the reductive region. However, three of these peaks are quite prominent and well separated, their height increasing with sequential addition of acid, indicating that they originate due to sequential reduction and protonation of **1Se**. We assume that **1Se** is somewhat unstable in the presence of $HBF_4{\cdot}Et_2O$ and that its partial degradation results in formation of redox-active species in solution, possibly accounting for the additional peaks seen in the CV of **1Se** in the presence of $HBF_4{\cdot}Et_2O$. Overall, a relatively large total current results, *ca.* 800 µA after addition of 10 equivalents of acid. Given the complex nature of the spectra, it is difficult to fully interpret likely mechanistic steps but it is assumed that **1Se** is first reduced at *ca.* −0.9 V followed by likely protonation to give $[HFe_3(CO)_9(\mu_3\text{-}Se)_2]$ (**1SeH**). Currents are relatively low at this potential, suggesting that while H_2 generation is possible, it is not favourable. A further reduction of **1SeH** appears to occur at *ca.* -1.5 V leading to formation of $[HFe_3(CO)_9(\mu_3\text{-}Se)_2]^-$ (**1SeH**$^-$) and if this binds a proton to yield $[H_2Fe_3(CO)_9(\mu_3\text{-}Se)_2]$ (**1SeH$_2$**), which regenerates **1Se** after H_2 loss. The current at this second potential is *ca.* 350 µA but at *ca.* -2.3 V, further H_2 generation ensues possibly associated with reduction to $[H_2Fe_3(CO)_9(\mu_3\text{-}Se)_2]^-$ (**1SeH$_2^-$**) and either H_2 loss (to generate **1Se**$^-$**)** or rapid protonation and H_2 loss to give **1SeH**. However, direct reduction of $HBF_4{\cdot}Et_2O$ by the electrode becomes prominent at this potential that also contributes to the catalytic currents. Liu and co-workers [15] previously studied the proton-reduction ability of $[Fe_3(CO)_9(\mu_3\text{-}S)_2]$ (**1S**) in CH_2Cl_2, finding that peak current of the first catalytic wave levels off upon addition of over three equivalents of acid, characteristic of a kinetically-controlled process; behaviour similar to that observed here.

We next considered the ability of **2S** and **2Se** to act as proton reduction catalysts (Fig. 8 and Fig S7) in CH_2Cl_2 using tosylic acid (*p*-TsOH) as the proton source. For **2S**, until addition of ca. 20 equivalents of acid there is no current uptake at the first reduction potential and even with 50 equivalents there is barely any catalysis at this potential. This shows that $[Fe_3(CO)_7(\mu_3\text{-}CO)(\mu_3\text{-}S)(\mu\text{-}dppm)]^-$ (**2S**)$^-$ is not catalytically active. After addition of ca. 20 equivalents of acid a new reduction peak appears at ca. -1.85 V, which we attribute to reduction of $[HFe_3(CO)_7(\mu_3\text{-}CO)(\mu_3\text{-}S)(\mu\text{-}dppm)]$ (**2SH**) formed in-situ. The peak height increases upon addition of further acid, suggesting generation of $[H_2Fe_3(CO)_7(\mu_3\text{-}CO)(\mu_3\text{-}S)(\mu\text{-}dppm)]$ (**2SH$_2$**), formed upon reduction of **2SH** followed by proton addition. At ca. 20 equivalents of acid, a third peak develops at ca. -2.10 V that continues to grow upon further addition of acid. We associate this with reduction of $[H_2Fe_3(CO)_7(\mu_3\text{-}CO)(\mu_3\text{-}S)(\mu\text{-}dppm)]$ (**2SH$_2$**) becoming competitive with H_2 loss. Thus, at higher acid concentrations the main H_2-generating pathway(s) is likely to occur from either $[H_2Fe_3(CO)_7(\mu_3\text{-}CO)(\mu_3\text{-}S)(\mu\text{-}dppm)]^-$ (**2SH$_2^-$**) or $[H_3Fe_3(CO)_7(\mu_3\text{-}CO)(\mu_3\text{-}S)(\mu\text{-}dppm)]$ (**2SH$_3$**), the latter being formed upon protonation of the anion. Behaviour of **2Se** is similar to that of **2S**. Even after addition of ca. 50 equivalents of acid there is virtually no electron uptake at the first reduction potential but after addition of ca. 20 equivalents, electron uptake begins at -1.85 V associated with reduction of $[HFe_3(CO)_7(\mu_3\text{-}CO)(\mu_3\text{-}Se)(\mu\text{-}dppm)]$ (**2SeH**). Soon after this (*ca.* 15 equivalents of acid) a further reduction wave appears at *ca.* -2.0 V associated with the formation of $[H_2Fe_3(CO)_7(\mu_3\text{-}CO)(\mu_3\text{-}Se)(\mu\text{-}dppm)]^-$(**2SeH$_2^-$**).

We next performed electrocatalytic studies of $[Fe_3(CO)_7(\mu_3\text{-}E)_2(\mu\text{-}dppm)]$ (**3**) under the same conditions as the studies on **2**

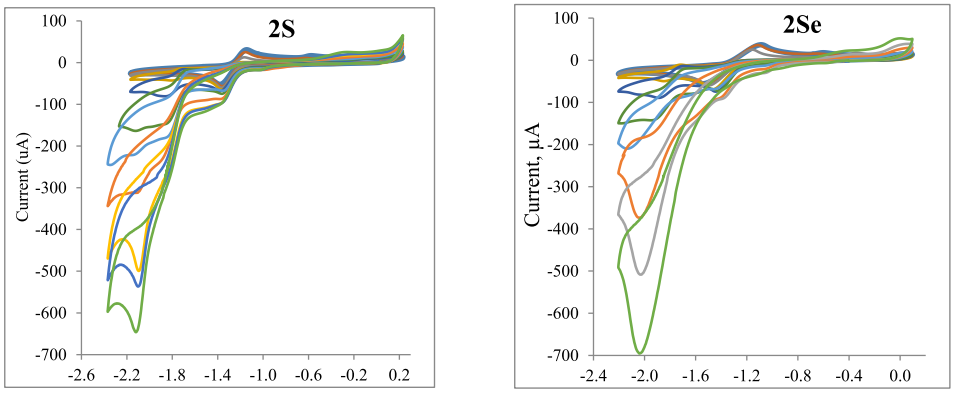

Fig. 8. CVs of (a) $[Fe_3(CO)_7(\mu_3\text{-}CO)(\mu_3\text{-}S)(\mu\text{-}dppm)]$ (**2S**) and (b) $[Fe_3(CO)_7(\mu_3\text{-}CO)(\mu_3\text{-}Se)(\mu\text{-}dppm)]$ (**2Se**) in CH_2Cl_2 in the absence and presence of 1–50 molar equivalents of *p*-TsOH (1 mM solution, supporting electrolyte $[NBu_4][PF_6]$, scan rate 0.25 V^{-1}, glassy carbon electrode, potential vs. Fc^+/Fc).

(Fig. 9). Kaiser and Knör have previously reported the electrocatalytic behaviour of **3S** in CH_2Cl_2 using CF_3CO_2H as the proton source [17]. Unlike **1** and **2**, bicapped **3** are protonated to some extent by strong acids in CH_2Cl_2 which means that a mixture of $[Fe_3(CO)_7(\mu_3\text{-}E)_2(\mu\text{-}dppm)]$ (**3**) and $[HFe_3(CO)_7(\mu_3\text{-}E)_2(\mu\text{-}dppm)]^+$ ($\mathbf{3}^+$) is present, the relative amounts of which depend on acid concentration, however except for at high acid concentrations the predominant species in solution is the neutral cluster, **3**. As generation of $[Fe_3(CO)_7(\mu_3\text{-}S)_2(\mu\text{-}dppm)]^-$ ($\mathbf{3S}^-$) leads to H_2 formation, this suggests that it can react with two equivalents of acid to afford $[H_2Fe_3(CO)_7(\mu_3\text{-}S)_2(\mu\text{-}dppm)]^+$ ($\mathbf{3SH_2^+}$). A new reduction wave of approximately equal intensity also appears at ca. -1.88 V and we associate this with reduction of $\mathbf{3SH_2^+}$ to afford $[H_2Fe_3(CO)_7(\mu_3\text{-}S)_2(\mu\text{-}dppm)]$ (**3SH$_2$**) which also releases H_2. After addition of ca. 10 equivalents of acid, a further new reduction peak appears at ca. -1.48 V, which we associate with reduction of $[HFe_3(CO)_7(\mu_3\text{-}S)_2(\mu\text{-}dppm)]^+$ ($\mathbf{3S}^+$), formed as a result of protonation of **3S**. After addition of ca. 20 acid equivalents, this peak does not change in size suggesting that H_2 loss is rate-determining from this species, a conclusion also made by Kaiser and Knör [17]. After addition of ca. 6 equivalents of acid a new reduction peak appears at ca. -2.1 V, and this grows with increasing acid concentration. This is possibly associated with reduction or rate-limiting loss of hydrogen from $[H_2Fe_3(CO)_7(\mu_3\text{-}S)_2(\mu\text{-}dppm)]$ (**3SH$_2$**) leading to competitive reduction to afford $[H_2Fe_3(CO)_7(\mu_3\text{-}S)_2(\mu\text{-}dppm)]^-$ ($\mathbf{3SH_2^-}$) that further protonates to give $[H_3Fe_3(CO)_7(\mu_3\text{-}S)_2(\mu\text{-}dppm)]$ (**3SH$_3$**) and releases hydrogen to generate $[HFe_3(CO)_7(\mu_3\text{-}S)_2(\mu\text{-}dppm)]$ (**3SH**).

Selenide-capped **3Se** behaves differently to **3S**. Even after addition of ca. 50 equivalents of acid no new reduction peaks are seen at less negative potentials than that for the formation of $[Fe_3(CO)_7(\mu_3\text{-}Se)_2(\mu\text{-}dppm)]^-$ ($\mathbf{3^-}$), suggesting that a protonated species does not exist in solution. The peak current of the first reduction potential increases gradually with the concentration of acid from the beginning, and this grows steadily upon further acid addition until around ca. 30 acid equivalents when it reaches a steady state, being associated with rate-limiting H_2 loss. After addition of ca. 10 equivalents of acid a new broad reduction peak appears at around -2.1 V and upon further acid addition, this grows and shifts to slightly more negative potentials but is always clearly positive of the direct reduction of acid by the electrode.

4. Summary and conclusions

We have reported comparative electrochemical and catalytic proton-reduction activity of three types of chalcogenide-capped clusters; $[Fe_3(CO)_9(\mu_3\text{-}E)_2]$ (**1**), $[Fe_3(CO)_7(\mu_3\text{-}CO)(\mu_3\text{-}E)(\mu\text{-}dppm)]$ (**2**) and $[Fe_3(CO)_7(\mu_3\text{-}E)_2(\mu\text{-}dppm)]$ (**3**) (E = S, Se). In general, the nature of the chalcogenide has little effect on the triiron core and consequent proton-reduction ability. Sulfide-capped clusters appear to be slightly more electron-rich than their selenide analogues, protonating to a greater extent in the presence of strong acids but being reduced at more negative reduction potentials. As expected, substitution of two carbonyls for the dppm ligand in **3** leads to shifts of the reduction potential to more negative values, but this is not mitigated by cluster core protonation (which lowers the reduction potential). More strongly electron-donating diphosphine ligands will need to be introduced in order to achieve the desired effect, and the introduction of dialkyl-substituted

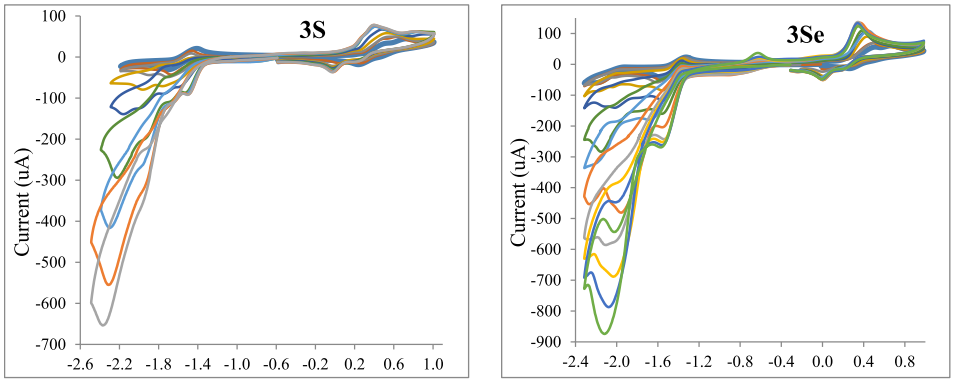

Fig. 9. CVs of complex (a) $[Fe_3(CO)_7(\mu_3\text{-}S)_2(\mu\text{-}dppm)]$ (**3S**) and (b) $[Fe_3(CO)_7(\mu_3\text{-}Se)_2(\mu\text{-}dppm)]$ (**3Se**) in CH_2Cl_2 in the absence and presence of up to 1–30 (**3S**) and up to 1–50 (**3Se**) molar equivalents of TsOH (1 mM solution, supporting electrolyte $[NBu_4][PF_6]$, scan rate 0.25 V s^{-1}, glassy carbon electrode, potential vs. Fc^+/Fc).

diphosphines such as $Cy_2PCH_2Cy_2$ into this type of cluster is currently under investigation. However, introduction of the diphosphine does stabilise the triiron centre towards CO loss, which has been shown to lead to complicated proton-reduction catalysis by $[Fe_3(CO)_9(\mu_3\text{-}S)_2]$ (**1S**) [15] and probably also accounts for the complex nature of the proton-reduction catalysis observed for **1Se** in the present study. While mono-chalcogenide clusters **2** are reduced at relatively low potentials (as compared to bicapped **3**), the corresponding 49-electron anions generated are not catalytically active, rendering **2** unattractive as proton-reduction catalysts. A further complication noted with these clusters was the Lewis basicity of the face-capping carbonyl, which ruled out using $HBF_4.Et_2O$ as a proton source. DFT calculations support formation of BF_3 adducts and also allow us to probe likely sites of protonation even when clusters do not protonate significantly with strong acids. Thus, protonation of **3S** is shown to occur across an iron-iron bonded vector and not across the open edge or at one of the capping sulfide ligands.

Acknowledgements

We thank the European Commission for the award of an Erasmus Mundus pre-doctoral fellowship (AR) and a postdoctoral fellowship (S.B-M) and the Commonwealth Scholarship Commission for the award of a scholarship to SG. GH and EN thank the Royal Society for an International Exchange Award. MGR thanks the Robert A. Welch Foundation (Grant B-1093-MGR) for financial support. Computational resources through the High-Performance Computing Services and CASCaM at the University of North Texas are acknowledged, and we thank Professor Michael B. Hall (Texas A&M University) for providing us a copy of his *JIMP2* program, which was used to prepare the geometry-optimized structures reported here.

Appendix A. Supplementary data

Supplementary data to this article can be found online at https://doi.org/10.1016/j.jorganchem.2018.10.018.

References

[1] W. McDowall, M. Eames, Energy Pol. 34 (2006) 1236–1250.
[2] J. Hetland, G. Mulder, Int. J. Hydrogen Energy 32 (2007) 736–747.
[3] M. Ball, M. Wietschel, Int. J. Hydrogen Energy 34 (2009) 615–627.
[4] K. Maeda, K. Teramura, D. Lu, T. Takata, N. Saito, Y. Inoue, K. Domen, Nature 440 (2006) 295.
[5] M. Grätzel, Nature 414 (2001) 338–344.
[6] O. Khaselev, J.A. Turner, Science 280 (1998) 425–427.
[7] L. Florin, A. Tsokoglou, T. Happe, J. Biol. Chem. 276 (2001) 6125–6132.
[8] M.W.W. Adams, Biochim. Biophys. Acta 1020 (1990) 115–145.
[9] S.P.J. Albracht, Biochem. Biophys. Acta 1188 (1994) 167–204.
[10] A. Volbeda, M.-H. Charon, C. Piras, E.C. Hatchikian, M. Frey, J.C. Fontecilla-Camps, Nature 373 (1995) 580–587.
[11] A. Volbeda, E. Garcin, C. Piras, A.L. de Lacey, V.M. Fernandez, E.C. Hatchikian, M. Frey, J.C. Fontecilla-Camps, J. Am. Chem. Soc. 118 (1996) 12989–12996.
[12] (a) D.J. Evans, C.J. Pickett, Chem. Soc. Rev. 32 (2003) 268–275;
(b) I.P. Georgakaki, L.M. Thomson, E.J. Lyon, M.B. Hall, M.Y. Darensbourg, Coord. Chem. Rev. 238–239 (2003) 255–266;
(c) T.B. Rauchfuss, Inorg. Chem. 43 (2004) 14–26;
(d) X. Liu, S.K. Ibrahim, C. Tard, C.J. Pickett, Coord. Chem. Rev. 249 (2005) 1641–1652;
(e) C. Tard, X. Liu, S.K. Ibrahim, M. Bruschi, L. De Gioia, S. Davies, X. Yang, L.-S. Wang, G. Sawers, C.J. Pickett, Nature 434 (2005) 610–613;
(f) L. Sun, B. Åkermark, S. Ott, Coord. Chem. Rev. 249 (2005) 1653–1663;
(g) J.-F. Capon, F. Gloaguen, F.Y. Pétillon, P. Schollhammer, J. Talarmin, Coord. Chem. Rev. 253 (9–10) (2009) 1476–1494;
(h) C. Tard, C.J. Pickett, Chem. Rev. 109 (2009) 2245–2274.
[13] (a) D. Fenske, J.F. Corrigan, in: P. Braunstein, L.A. Oro, P.R. Raithby (Eds.), Metal Clusters in Chemistry, vol. 3, Wiley-VCH, Weinheim, 1999, p. 1302;
(b) W.A. Herrmann, Angew. Chem., Int. Ed. Engl. 25 (1986) 56–76;
(c) D. Fenske, J. Ohmer, J. Hachgenei, K. Merzweiler, Angew. Chem., Int. Ed. Engl. 27 (1988) 1277–1296;
(d) N.A. Compton, R.J. Errington, N.C. Norman, Adv. Organomet. Chem. 31 (1990) 91–182;
(e) D.F. Shriver, H.D. Kaesz, R.D. Adams, The Chemistry of Metal Cluster Complexes, Wiley-VCH, New York, 1990;
(f) L.C. Roof, W. Kolis, Chem. Rev. 93 (1993) 1037–1080;
(g) H. Vahrenkamp, Angew. Chem., Int. Ed. Engl. 14 (1975) 322–329;
(h) R.D. Adams, M. Tasi, J. Cluster Sci. 3 (1990) 249–267;
(i) M.G. Richmond, Coord. Chem. Rev. 241 (2003) 273–294;
(j) M.G. Richmond, Coord. Chem. Rev. 248 (2004) 881–901;
(k) M.A. Ansari, J.A. Ibers, Coord. Chem. Rev. 100 (1990) 223–266;
(l) M.G. Kanatzidis, S.-P. Huang, Coord. Chem. Rev. 130 (1994) 509–621;
(m) P. Mathur, Adv. Organomet. Chem. 41 (1997) 243–314;
(n) M. Shieh, J. Cluster Sci. 10 (1999) 3–36.
[14] C.A. Mebi, K.E. Brigance, R.B. Bowman, J. Braz. Chem. Soc. 23 (2012) 186–189.
[15] Z. Li, X. Zeng, Z. Niu, X. Liu, Electrochim. Acta 54 (2009) 3638–3644.
[16] W. Gao, J. Sun, M. Li, T. Åkermark, K. Romare, L. Sun, B. Åkermark, Eur. J. Inorg. Chem. 7 (2011) 1100–1105.
[17] M. Kaiser, G. Knör, Eur. J. Inorg. Chem. 25 (2015) 4199–4206.
[18] S. Ghosh, G. Hogarth, K.B. Holt, S.E. Kabir, A. Rahaman, D.G. Unwin, Chem. Commun. 47 (2011) 11222–11224.
[19] A. Rahaman, S. Ghosh, D.G. Unwin, S. Basak-Modi, K.B. Holt, S.E. Kabir, E. Nordlander, M.G. Richmond, G. Hogarth, Organometallics 33 (2014) 1356–1366.
[20] S. Ghosh, K.B. Holt, S.E. Kabir, M.G. Richmond, G. Hogarth, Dalton Trans. 44 (2015) 5160–5169.
[21] S. Ghosh, G. Hogarth, J. Organomet. Chem. 851 (2017) 57–67.
[22] S. Ghosh, S. Basak-Modi, M.G. Richmond, E. Nordlander, G. Hogarth, Inorg. Chim. Acta. 480 (2018) 47–53.
[23] A. Rahaman, G.C. Lisensky, D.A. Tocher, M.G. Richmond, G. Hogarth, E. Nordlander, J. Organomet. Chem. 867 (2018) 381–390.
[24] J.-P. Li, Y.-C. Shi, Inorg. Chim. Acta. 482 (2018) 77–84.
[25] (a) M.D. Rail, L.A. Berben, J. Am. Chem. Soc. 133 (2011) 18577–18579;
(b) A.D. Nguyen, M.D. Rail, M. Shanmugam, J.C. Fettinger, L.A. Berben, Inorg. Chem. 52 (2013) 12847–12854.
[26] C. Tard, X. Liu, D.L. Hughes, C.J. Pickett, Chem. Commun. (2005) 133–135.
[27] M.H. Cheah, C. Tard, S.J. Borg, X. Liu, S.K. Ibrahim, C.J. Pickett, S.P. Best, J. Am. Chem. Soc. 129 (2007) 11085–11092.
[28] H. Adams, S.C.M. Agustinho, K. Chomka, B.E. Mann, S. Smith, C. Squires, S.E. Spey, Can. J. Chem. 79 (2001) 760–774.
[29] C.H. Wei, L.F. Dahl, Inorg. Chem. 4 (1965) 493–499.
[30] W. Hieber, J. Gruber, Z. Anorg. Allg. Chem. 296 (1958) 91–103.
[31] A.X.S. Bruker, APEX2 - Software Suite for Crystallographic Programs, Bruker AXS, Inc., Madison, WI, USA, 2009.
[32] CrysAlisPro Agilent, Agilent Technologies inc., Yarnton, Oxfordshire, England, 2014.
[33] G.M. Sheldrick, Acta Crystallogr. A64 (2008) 112–122.
[34] L. Palatinus, G. Chapuis, J. Appl. Cryst. 40 (2007) 786–790.
[35] G.M. Sheldrick, SADABS - Bruker Nonius Scaling and Absorption Correction, Bruker, AXS, Inc., Madison, Wisconsin, USA, 2012.
[36] M.J. Frisch, G.W. Trucks, H.B. Schlegel, G.E. Scuseria, M.A. Robb, J.R. Cheeseman, G. Scalmani, V. Barone, B. Mennucci, G.A. Petersson, H. Nakatsuji, M. Caricato, X. Li, H.P. Hratchian, A.F. Izmaylov, J. Bloino, G. Zheng, J.L. Sonnenberg, M. Hada, M. Ehara, K. Toyota, R. Fukuda, J. Hasegawa, M. Ishida, T. Nakajima, Y. Honda, O. Kitao, H. Nakai, T. Vreven, J.A. Montgomery Jr., J.E. Peralta, F. Ogliaro, M. Bearpark, J.J. Heyd, E. Brothers, K.N. Kudin, V.N. Staroverov, R. Kobayashi, J. Normand, K. Raghavachari, A. Rendell, J.C. Burant, S.S. Iyengar, J. Tomasi, M. Cossi, N. Rega, J.M. Millam, M. Klene, J.E. Knox, J.B. Cross, V. Bakken, C. Adamo, J. Jaramillo, R. Gomperts, R.E. Stratmann, O. Yazyev, A.J. Austin, R. Cammi, C. Pomelli, J.W. Ochterski, R.L. Martin, K. Morokuma, V.G. Zakrzewski, G.A. Voth, P. Salvador, J.J. Dannenberg, S. Dapprich, A.D. Daniels, O. Farkas, J.B. Foresman, J.V. Ortiz, J. Cioslowski, D.J. Fox, Gaussian 09, Revision A.02, Gaussian, Inc., Wallingford CT, 2009.
[37] A.D. Becke, J. Chem. Phys. 98 (1993) 5648–5652.
[38] C. Lee, W. Yang, R.G. Parr, Phys. Rev. B (1988) 785–789, 37.
[39] (a) M. Dolg, U. Wedig, H. Stoll, H. Preuss, J. Chem. Phys. 86 (1987) 866–872;
(b) S.P. Walch, C.W. Bauschlicher, J. Chem. Phys. 78 (1983) 4597–4605.
[40] (a) G.A. Petersson, A. Bennett, T.G. Tensfeldt, M.A. Al-Laham, W.A. Shirley, J. Mantzaris, J. Chem. Phys. 89 (1988) 2193–2218;
(b) G.A. Petersson, M.A. Al-Laham, J. Chem. Phys. 94 (1991) 6081–6090.
[41] A.E. Reed, L.A. Curtiss, F. Weinhold, Chem. Rev. 88 (1988) 899–926.
[42] K.B. Wiberg, Tetrahedron 24 (1968) 1083–1096.
[43] (a) M.B. Hall, R.F. Fenske, JIMP2, version 0.091, a free program for the visualization and manipulation of molecules, Inorg. Chem. 11 (1972) 768–779;
(b) J. Manson, C.E. Webster, M.B. Hall, Texas A&M University, College Station, TX, 2006. http://www.chem.tamu.edu/jimp2/index.html.
[44] (a) L. Markó, T. Madach, H. Vahrenkamp, J. Organomet. Chem. 190 (1980) C67–C70;
(b) R.D. Adams, J.E. Babin, M. Tasi, Organometallics 7 (1988) 219–227;
(c) R.D. Adams, I.T. Horvath, H.S. Kim, Organometallics 3 (1984) 548–558;
(d) C. Graiff, G. Predieri, A. Tiripicchio, Eur. J. Inorg. Chem. 9 (2003) 1659–1668.
[45] (a) S.N. Konchenco, A.V. Virovets, S.V. Thachev, Zh. Strukt. Khim. 39 (1998) 894;
(b) A.V. Virovets, S.N. Konchenko, D. Fenske, J. Struc. Chem. 43 (2002)

694–696.
[46] S.E. Kabir, G. Hogarth, Coord. Chem. Rev. 253 (2009) 1285–1315.
[47] G. Hogarth, N.J. Taylor, A.J. Carty, A. Meyer, J. Chem. Soc. Chem. Commun. (1988) 834–836.
[48] D. Cauzzi, C. Graiff, M. Lanfranchi, G. Predieri, A. Tiripicchio, J. Organomet. Chem. 536–537 (1997) 497–507.
[49] (a) F. Gloaguen, J.D. Lawrence, T.B. Rauchfuss, J. Am. Chem. Soc. 123 (2001) 9476–9477;
(b) L. Schwartz, G. Eilers, L. Eriksson, A. Gogoll, R. Lomoth, S. Ott, Chem. Commun. (2006) 520–522;
(c) F.I. Adam, G. Hogarth, I. Richards, J. Organomet. Chem. 692 (2007) 3957–3968;
(d) F.I. Adam, G. Hogarth, S.E. Kabir, I. Richards, C. R. Chim. 11 (2008) 890–905;
(e) I.P. Georgakaki, M.L. Miller, M.Y. Darensbourg, Inorg. Chem. 42 (2003) 2489–2494.
[50] B.E.R. Schilling, R. Hoffmann, J. Am. Chem. Soc. 101 (1979) 3456–3467.
[51] T. Madach, H. Vahrenkamp, Chem. Ber. 114 (1981) 505–512.